Analyst

ROYAL SOCIETY OF CHEMISTRY

PAPER

View Article Online
View Journal | View Issue

Cite this: *Analyst*, 2022, **147**, 4845

Switchable inhibitory behavior of divalent magnesium ion in DNA hybridization-based gene quantification†

Hyowon Jin,[a] Hyun Jeong Lim,[a,b] Mark R. Liles,[c] Beelee Chua *[d] and Ahjeong Son *[a]

Contrary to the understanding that divalent cations only result in under-estimation of gene quantification *via* DNA hybridization-based assays, we have discovered that Mg^{2+} could cause either under or over-estimation at different concentrations. Its switchable inhibitory behavior is likely due to its rigid first solvation (hydrated) shell and hence it is inclined to form non-direct binding with DNA. At low concentrations, it caused under-estimation by occupying the hybridization sites. At high concentrations, it caused probe, signaling and target DNA to aggregate non-specifically *via* Coulomb forces. By quantifying target DNAs at a range of Mg^{2+} concentrations using a gene quantification assay (NanoGene assay), a Mg^{2+} inflection concentration of ~10^{-3} M was observed for both target ssDNA and dsDNA. Field emission scanning electron microscopy (FE-SEM), energy dispersive X-ray spectroscopy (EDS), and Fourier transform infrared spectroscopy (FT-IR) were employed to observe Mg^{2+}-induced non-specific binding in the complexes that mimicked the presence of target DNA. Together with two other divalent cations Ca^{2+} and Cu^{2+}, they were further examined *via* zeta potential measurements as well as NanoGene assay. This study revealed the importance of Mg^{2+} in achieving accurate gene quantification. Through a better mechanistic understanding of this phenomenon, it will be possible to develop strategies to mitigate the impact of Mg^{2+} on DNA hybridization-based gene quantification.

Received 19th July 2022,
Accepted 15th September 2022

DOI: 10.1039/d2an01164f

rsc.li/analyst

1. Introduction

Gene quantification using DNA hybridization-based assays is invaluable to gain insight into the dynamics of microbial communities and the presence of pathogens in environmental samples. These molecular tools can help to address multitudes of environmental microbially driven challenges and conundrums related to public health, agriculture, and climate change.[1–4] The applications of DNA hybridization-based assays include the early detection of specific pathogenic bacteria, early warning of imminent cyanobacterial bloom, and biosequestration of carbon by soil microbial communities.[5–9]

However, these assays are often susceptible to inhibitory compounds (inhibitors) that co-exist with the samples.[10–12] These inhibitors would hinder DNA hybridization and result in quantification under-estimation. Typically, its severity would be exacerbated as the concentration of inhibitors is increased.[13,14] It is useful to recall that DNA hybridization-based assays rely on the hybridization between the target DNA and the probe as well as signaling DNAs (Fig. 1a). The amount of target DNA is quantified by the relative amount of signaling DNA to the probe DNA. This can be measured *via* fluorescence labels or otherwise. With the presence of inhibitors, such as humic acids[15–19] and divalent cations,[12,20,21] the target DNA would not be able to hybridize with the probe and signaling DNAs (Fig. 1b). This results in quantification under-estimation.

In this study, we have discovered that divalent magnesium (Mg^{2+}) does not behave like any of these inhibitors. As its concentration transverse through the environmentally relevant range, the gene quantification switched from under-estimation to over-estimation. At high concentrations, while preventing probe and signaling DNAs from coming together *via* hybridization, it brought them together instead *via* Coulomb forces (Fig. 1c). The counter-intuitive observation at high concen-

[a]*Department of Environmental Science and Engineering, Ewha Womans University, 52 Ewhayeodae-gil, Seodaemun-gu, Seoul 03760, Republic of Korea. E-mail: ason@ewha.ac.kr, ahjeong.son@gmail.com; Tel: +82 (2) 3277-3339*
[b]*Department of Chemical and Environmental Engineering, Yale University, New Haven, CT 06511, USA*
[c]*Department of Biological Sciences, Auburn University, Auburn, AL 36849, USA*
[d]*School of Electrical Engineering, Korea University, 145 Anam-ro, Seongbuk-gu, Seoul 02841, Republic of Korea. E-mail: bchua@korea.ac.kr, chuabeelee@gmail.com; Tel: +82 (2) 3290-4639*

† Electronic supplementary information (ESI) available. See DOI: https://doi.org/10.1039/d2an01164f

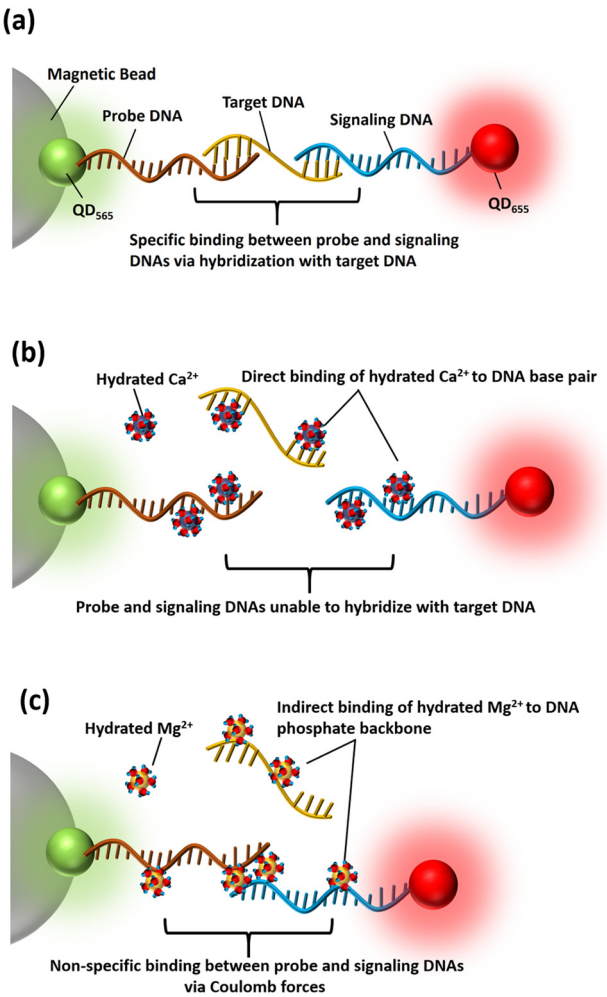

Fig. 1 Schematic of (a) specific detection of target DNA by the NanoGene assay. (b) Singular inhibition by Ca^{2+} *via* direct binding to base pair. (c) Switchable inhibition by Mg^{2+} *via* indirect binding to phosphate backbone.

trations therefore became that of over-estimation instead of the usual under-estimation.

In particular, the inflection concentration of Mg^{2+} (for a given target DNA concentration) where the switching occurs would be of interest and it was investigated *via* a well-established gene quantification assay (NanoGene assay).[5–7,11,22–25] Briefly, the NanoGene assay consisted of two complexes: (i) magnetic bead-quantum dot-probe DNA complex (MB-QD_{565}-probe DNA) and (ii) signaling DNA-quantum dot complex (signaling DNA-QD_{655}). The successful hybridization with the target DNA would bring these two complexes together. The fluorescence ratio between QD_{655} and QD_{565} would inform us of the target DNA concentration. The details pertaining to the NanoGene assay is presented in ESI.† Two different types of target DNA (ssDNA and dsDNA) would be employed.

In addition, field emission scanning electron microscopy (FE-SEM), energy dispersive X-ray spectroscopy (EDS), and Fourier transform infrared spectroscopy (FT-IR) were employed to observe Mg^{2+}-induced non-specific binding in the complexes that mimicked the presence of target DNA. Together with two other divalent cations Ca^{2+} and Cu^{2+}, they were further examined *via* zeta potential measurements as well as NanoGene assay at varying concentrations. In this way, we could gain further understanding of Mg^{2+} as a switchable inhibitor that can result in experimental biases that distort the assay results in unexpected ways. It will be critical for the future formulation of compensation schemes to enable more accurate gene quantification in Mg^{2+} laden samples. It will also allow us to identify other switchable inhibitors in gene quantification assays in general.

2. Materials and methods

2.1. Preparation of divalent cations solution

The Mg^{2+} stock solution (10 M) was prepared by dissolving magnesium chloride hydrate ($MgCl_2{\cdot}6H_2O$, 10.165 g, Daejung Co. Ltd, Korea) and magnesium sulfate hydrate ($MgSO_4{\cdot}7H_2O$, 12.325 g, Daejung) in 10 mL of autoclaved deionized water.[26] The Ca^{2+} stock solution (10 M) was prepared by dissolving 58.8 g of calcium chloride hydrate ($CaCl_2{\cdot}2H_2O$, Daejung) in 40 mL of autoclaved deionized water. The Cu^{2+} stock solution (2 M) was prepared by dissolving 5.0 g of copper sulfate hydrate ($CuSO_4{\cdot}5H_2O$, Daejung) in 10 mL of autoclaved deionized water. The autoclaved deionized water was prepared by autoclaving Millipore deionized water and followed by filter-sterilization using nylon membrane filter (Chmlab, Barcelona, Spain) with a pore size of 0.45 μm. The stock solutions of Mg^{2+}, Ca^{2+}, and Cu^{2+} (final concentrations of 10^{-5} to 10^{0} M) was added prior to the DNA hybridization (180 μL) during the NanoGene assay. The DNA hybridization was performed overnight at room temperature in a 2.0 mL Eppendorf tube. A negative control was prepared without adding the stock solutions of Mg^{2+}, Ca^{2+}, and Cu^{2+}.

2.2. NanoGene assay as gene quantification assay

The detailed procedures for the NanoGene assay were described in previous studies.[5,6,12,22] Briefly, probe and signaling DNAs (Bioneer, Daejeon, Korea) were covalently conjugated with quantum dots (QD_{565} and QD_{655}, Invitrogen, Carlsbad, CA) and MB (Dynabead M270 Amine, Invitrogen) with the aid of EDC (ethylcarbodiimide, Sigma-Aldrich, Saint-Louis, MO) and NHS (*N*-hydroxysuccinimide, Sigma-Aldrich). Both probe and signaling DNAs with attached quantum dots were subjected to DNA hybridization with the target DNA. The target DNA could be in the form of ssDNA,[6,10,22] dsDNA PCR amplicon,[22] shredded gDNA,[5] or lysed soil sample.[12] The complexes were magnetically separated and washed with 0.1 M phosphate buffer three times to remove unbound or non-specifically bound complexes. The fluorescence intensity of QD_{565} and QD_{655} were measured using a spectrofluorometer (Molecular Devices, SpectraMax M2, Sunnyvale, USA) at excitation wavelength of 360 nm and emission wavelengths of 570 and 660 nm. The fluorescence ratio (*i.e.* QD_{655}/QD_{565}, relative fluo-

rescence unit or RFU) and the normalized fluorescence percentage (*i.e.* fluorescence ratio of sample/fluorescence ratio of blank × 100 or %) were used to quantify the target DNA for comparison. All experiments were performed in triplicate.

2.3. Preparation of ssDNA and dsDNA as target DNA

Two types of DNA templates (synthetic ssDNA and dsDNA PCR amplicon) were used as target DNAs in this study. As previously described,[5,21,22] ssDNA oligonucleotide with a sequence that is a part of the *mcy*D gene (5′-TTA GAG CAT CCA TGA AAG CAT TAG CTG CGG CAT AAT TAC TTT GAC CAG GC-3′) was synthesized. The *mcy*D gene encodes microcystin synthetase and is specific to *Microcystis aeruginosa*, a well-known cyanobacteria responsible for harmful aquatic blooms.

The dsDNA PCR amplicon was prepared in accordance with that reported in a previous study.[22] *Microcystis aeruginosa* strain UTEX 2388 was purchased from the Culture Collection of Algae at the University of Texas, USA. The strain UTEX 2388 is known for the production of the toxin, microcystin.[27] The *Microcystis aeruginosa* was cultured at room temperature with an agitation of 100 rpm and under continuous illumination of 20 000 lux (30 W, EFQU30EX-D, Incheon, South Korea) in modified Bold 3N medium. The algal culture was collected in a sterile 15 mL Falcon tube by centrifugation at 3000 rpm for 30 min. The genomic DNA was extracted in duplicate using a Qiagen DNeasy PowerSoil kit (Qiagen, Germany). It was subsequently eluted in 100 μL of the elution buffer and stored at −20 °C. The DNA extracts were quantified using a NanoDrop™ 1000 spectrophotometer (Thermo Scientific, Wilmington, USA).

The microcystin toxin synthetase *mcyD* gene fragment was amplified from the gDNA of *Microcystis aeruginosa* by PCR using primers *mcyD*F2 (5′-GGT TCG CCT GGT CAA AGT AA-3′) and *mcyD*R2 (5′-CCT CGC TAA AGA AGG GTT GA-3′). The reaction mixture was prepared in a 50 μL total volume containing 400 nM of each primer, 1× Mg-free PCR buffer (Takara, Shiga, Japan), 20 mM $MgCl_2$, 200 nM dNTPs, 2 U of *Tag* polymerase (Takara), and 20 ng of DNA template. The PCR amplification consisted of an initial denaturation for 5 min at 95 °C, 50 cycles of for 30 s at 94 °C, 60 s at 55 °C (optimized in this study), and 30 s at 72 °C, with a final extension of 15 min at 72 °C.[28] In order to confirm the size of PCR product (297 bp), PCR product was loaded into a 1.5% agarose gel and the DNA band was visually inspected under UV illumination using gel imaging system (Molecular Imager Gel Doc™ XR+ System, Bio-rad, Hercules, CA, USA) after staining the gel with 10 mg mL^{-1} of ethidium bromide (Bio-rad) in 0.5× TBE (Bioneer, Daejeon, Korea). The concentration of the PCR product was measured at λ = 260 nm using NanoDrop™ 1000 spectrophotometer. The dsDNA PCR fragment (297 bp, 10^9 *mcyD* gene copy number) was denatured at 95 °C for 5 min prior to DNA hybridization in a vial as part of the NanoGene assay.[29]

2.4. Fourier transform infrared spectroscopy (FT-IR)

FT-IR analysis was performed to observe the changes in bonding between Mg^{2+} only, target DNA with Mg^{2+} as well as MB-QD_{565}-probe DNA complex at different Mg^{2+} concentrations. The absorbance was measured using Agilent Cary 630 Fourier Transform Infrared (FT-IR) spectrometer in the range of 650–1800 cm^{-1} (fingerprint to double bond region) assisted by the ZnSe ATR module at room temperature. The target DNA was in the form of dsDNA with 10^{12} *mcy*D gene copy number. The Mg^{2+} stock solution (0, 10^{-4}, 10^{-2}, and 10^0 M as final concentrations) was added to the DNA and complexes (total volume of 50 μL). The negative control added with ultrapure water instead of Mg^{2+} stock solution. The samples were dried prior to the FT-IR analysis.

2.5. Effect of Mg^{2+} on different complexes

The three complexes used in the study were (i) MB-QD_{565}-probe DNA, (ii) QD_{655}-signaling DNA, and (iii) MB-QD_{565}-probe DNA + signaling DNA-QD_{655}:

(i) MB-QD_{565}-probe DNA complex: MB (80 μL, 2×10^9 beads mL^{-1}) and 64 μL of QD_{565} (64 μL, 2 μM) was covalently conjugated by 500 μL EDC & NHS mixture and 700 μL MES buffer (0.1 M) in the Mixmate shaker (1200 rpm, Eppendorf, Hamburg, Germany) at room temperature for 2 h. The probe DNA (40 μL, 100 μM) was further added and incubated for another covalent linkage with QD_{565} and the complex was then washed with 0.1 M phosphate buffer (pH = 7.4) four times. The washed complex was suspended in 1856 μL ultrapure water and 144 μL Mg^{2+} stock solutions to make 10^{-5}, 10^{-4}, 10^{-3}, 10^{-2}, 10^{-1}, and 10^0 M Mg^{2+} as final concentrations in 2 mL volume. The complex was then subjected to fluorescence and zeta potential measurement after 10 min.

(ii) The signaling DNA-QD_{655} complex: QD_{655} (64 μL, 2 μM) and signaling DNA (12.8 μL, 100 μM) was covalently conjugated by 100 μL EDC & NHS mixture and 300 μL borate buffer (10 mM) in the Mixmate shaker at room temperature for 2 h. $NaBH_4$ solution (SSC buffer based)[25] was added for the passivation of functional groups and centrifuged (20 min, 14 000 rpm). After washing 2 times, the spin down complex was resuspended in 1856 μL ultrapure water and 144 μL Mg^{2+} stock solutions to make 10^{-5}, 10^{-4}, 10^{-3}, 10^{-2}, 10^{-1}, and 10^0 M Mg^{2+} as final concentrations in 2 mL volume. The complex was then subjected to fluorescence and zeta potential measurement after 10 min.

(iii) Samples containing both MB-QD_{565}-probe DNA and signaling DNA-QD_{655}: firstly, MB-QD_{565}-probe DNA and signaling DNA-QD_{655} complexes were prepared separately as described in (1) and (2). Both complexes was then combined with DIG hyb easy buffer, ultrapure water, and Mg^{2+} solutions to make 10^{-5}, 10^{-4}, 10^{-3}, 10^{-2}, 10^{-1}, and 10^0 M Mg^{2+} as final concentrations in 2 mL volume. The complex was then subjected to fluorescence and zeta potential measurement after 10 min.

2.6. Fluorescence measurement

Fluorescence measurement was performed for different complexes in the presence of Mg^{2+} (10^{-5}, 10^{-4}, 10^{-3}, 10^{-2}, 10^{-1}, and 10^0 M). (i) MB-QD_{565}-probe DNA complex with Mg^{2+} was subjected to the fluorescence measurement at λ_{ex} = 360 nm and λ_{em} = 570 nm using a SpectraMax M2 spectrofluorometer

(Molecular Devices, Sunnyvale, USA). (ii) Signaling DNA-QD_{655} complex with Mg^{2+} were measured at λ_{ex} = 360 nm and λ_{em} = 660 nm. (iii) MB-QD_{565}-probe DNA + signaling DNA-QD_{655} complexes with Mg^{2+} were measured at λ_{ex} = 360 and λ_{em} = 570 and 660 nm. For fluorescence measurement, 200 μL of each sample was used. All measurements were taken 10 min after Mg^{2+} addition, and each sample was measured four times.

2.7. Zeta potential measurement

Zeta potential measurement was performed to observe the binding behaviors for each complex by the addition of Mg^{2+}. It was performed by laser Doppler velocimetry using the zeta potential analyzer ELSZ-2000 (Otsuka Electronics, Osaka, Japan). The zeta potential was measured for above 3 complexes (MB-QD_{565}-probe DNA, signaling DNA-QD_{655}, and MB-QD_{565}-probe DNA + signaling DNA-QD_{655}) at different Mg^{2+} concentrations (10^{-5}, 10^{-4}, 10^{-3}, 10^{-2}, 10^{-1}, and 10^{0} M) in water. To facilitate the measurement of the zeta potential, the total volume was adjusted to 2 mL with ultrapure distilled water (UltraPure™ DNase/RNase-Free Distilled Water, Invitrogen). Two mL of the sample was transferred to the Otsuka zeta flow cells and measured. Zeta potential measurement was performed four times for each sample.

2.8. High resolution field emission scanning electron microscopy (HR FE-SEM)

MB-QD_{565}-probe DNA + signaling DNA-QD_{655} complex with different Mg^{2+} concentration was subjected to HR FE-SEM analysis. The sample was first centrifuged for 10 min and the supernatant was discarded. It subsequently dried at the room temperature. The powder form of samples was analyzed using HR FE-SEM (SU8220, Hitachi, Japan; equipped at KBSI Western Seoul Center in Korea) at an accelerating voltage of 15.0 kV. In addition, the elemental composition was analyzed by energy dispersive X-ray spectroscopy (EDS).

3. Results and discussion

3.1. FE-SEM and EDS observations

The magnetic beads (MB) were highly visible in a FE-SEM the image but the quantum dots (QD) as well as probe and signaling DNAs were not visible individually due to the nanoscale sizes of QD and DNAs (Fig. 2a). Nonetheless, in the absence of Mg^{2+}, the magnetic beads (MB) appeared to be relatively well-dispersed and it suggested that there was no increase in binding or aggregation between individual MB-QD_{565}-probe DNA. There was also no indication of aggregation facilitated by QD_{655}-signaling DNA. This is consistent with the understanding that MB-QD_{565}-probe DNA and QD_{655}-signaling DNA complexes do not possess the affinity for each other.

However, in the presence of Mg^{2+} (10^{-5}, 10^{-4}, 10^{-2} and 10^{0} M) there were noticeable aggregation in all four concentrations of Mg^{2+} (Fig. 2b–e). At 10^{-5} M Mg^{2+}, the MB-QD_{565}-probe DNA complexes aggregated more as compared to that shown in the absence of Mg^{2+} (Fig. 2a). As the concentration of Mg^{2+} increased to 10^{-4} M, secondary aggregation may have appeared on the surface of the magnetic beads (Fig. 2c), which became more visible at 10^{-2} as well as 10^{0} M Mg^{2+} (Fig. 2d and e).

The nature of the secondary aggregation, presumably that by QD_{655}-signaling DNA complexes onto the QD_{565}-probe DNA at the MB's surface, was further examined based on EDS results (Fig. 3a–c). As expected, the magnetic beads (MB) coincided with the Fe distribution (Fig. 3a). The remaining elements were Cd, Zn, and Se, presumably from the quantum dots, and there was no Mg^{2+} present.

As mentioned earlier with the presence of Mg^{2+} at 10^{-2} M, secondary aggregation (*denoted as "SA" in the image*) became visible (Fig. 3b). The distribution of Fe still corresponded to that of the magnetic beads (MB). However, the distribution of Mg corresponded to that of the observed secondary aggregation. Similarly, at 10^{-2} M Mg^{2+}, the distribution of Fe corresponded to that of magnetic beads (MB), while that of Mg corresponded to that of secondary aggregation (Fig. 3c). With these observations, it is reasonable to suggest that there was Mg^{2+}-induced aggregation. More specifically, since Mg^{2+} could not have formed visible microstructures by itself, the only other possibility is that it was binding *en* masse to QD_{655}-signaling DNA and QD_{565}-probe DNA at the MB's surface. Since it was mentioned earlier that the Mg^{2+} bond with DNA could be indirect and dominated by Coulomb forces, it is consistent that these Coulomb forces would be sufficiently large to pull the complexes together to form large visible aggregates as observed in the FE-SEM and EDS analyses.

3.2. FT-IR absorbance spectrum of target DNA and MB-QD_{565}-probe DNA complex in the presence of Mg^{2+}

A broad peak was observed by FT-IR absorbance spectroscopy at ~1630 cm^{-1} for all three concentrations and it corresponded to that of HOH bending vibration band of $MgSO_4 \cdot 7H_2O$ (Fig. 4a and b).[30] However, the broad peak at ~1100 cm^{-1} was only observed for the concentration of 10^{0} M and not for the lower concentrations (10^{-2} and 10^{-4} M). It corresponded to the characteristic of SO_4^{-2} stretching vibration band in $MgSO_4 \cdot 7H_2O$.[30–33] Note that in supersaturated $MgSO_4$ where simple contact ion pairs are dominant, there seems to be a red shift of the broad peak associated with SO_4^{-2} from ~1100 cm^{-1} to ~1005 cm^{-1}. With further dilution such that Mg^{2+} and SO_4^{-2} exist as double solvent-separated ion pairs or solvent-shared ion pairs, the SO_4^{-2} peak undergoes further red shifts.[34] Therefore, it seemed to suggest that there could have been $MgSO_4 \cdot 7H_2O$ precipitation at a concentration of 10^{0} M.

The target DNA (dsDNA) yielded peaks at 851, 921, 992, 1036, and 1109 cm^{-1}, which appeared to be attributed to that of DNA structure (Fig. 4c and d).[35–40] In particular, 860, 1050, and 1100 cm^{-1} may be attributed to PO_2^- and sugar-phosphate backbone modes in B-DNA;[35] 893, 1069, and 1089 cm^{-1} may be attributed to the sugar-phosphate stretching bands in B-DNA;[36] 929 and 1080 cm^{-1} may be attributed to that for DNA and PO_2^- DNA;[37] 1250–1500 cm^{-1} may be attributed to that of DNA base-sugar vibration. With the increase of the concentration from 0 to 10^{-2} M, the peak at ~1036 cm^{-1} decreased.

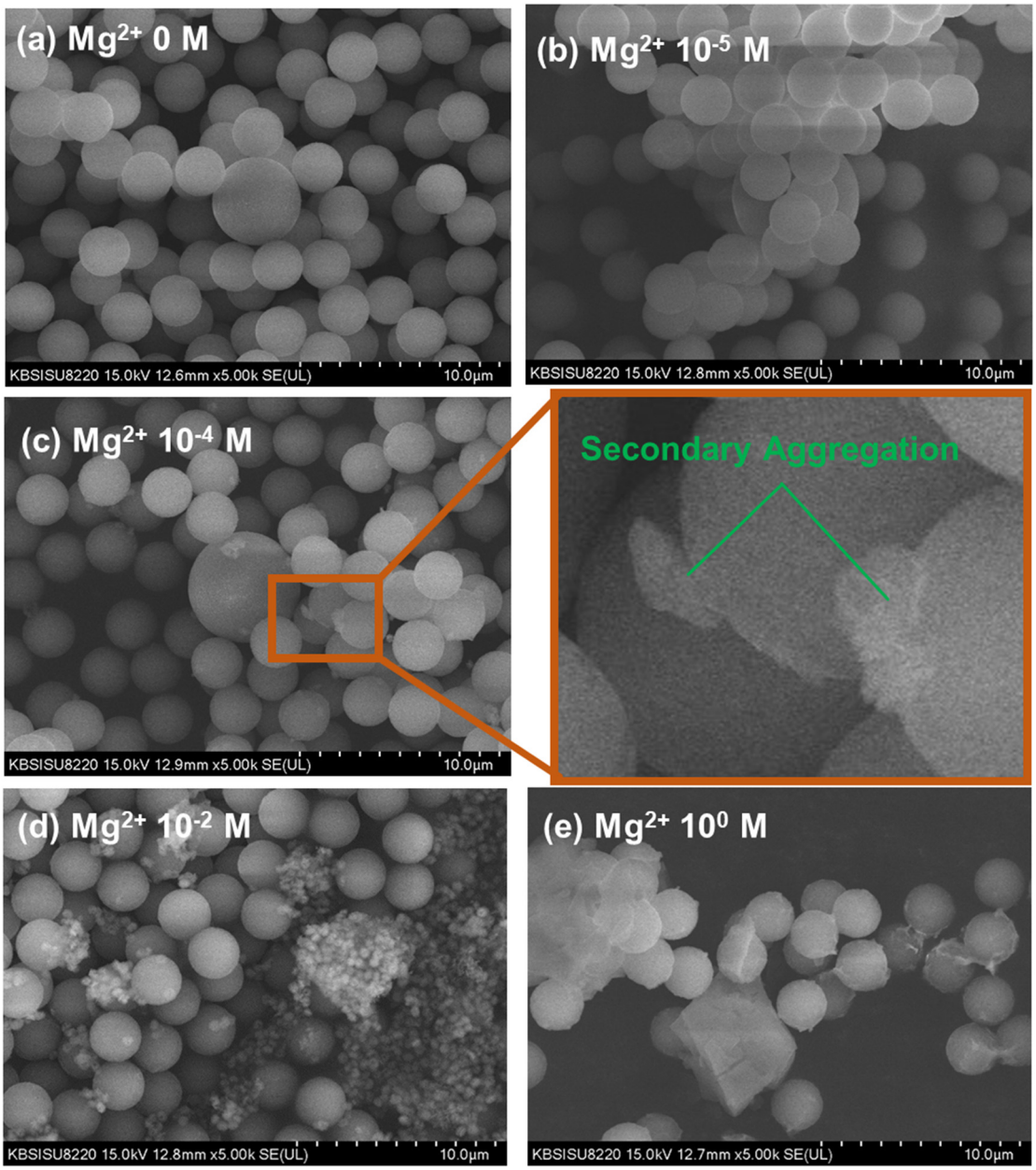

Fig. 2 FE-SEM images of MB-QD_{565}-probe DNA + QD_{655}-signaling DNA in the presence of Mg^{2+} ions of (a) 0 M, (b) 10^{-5} M, (c) 10^{-4} M, (d) 10^{-2} M, and (e) 10^{-0} M. Secondary aggregation was observed on the surfaces of the magnetic beads (MB), as shown in the zoom-in picture of (c).

Since it is likely to be attributed that of sugar-phosphate stretching bands, it would suggest that there was less stretching of the sugar-phosphate backbone as the Mg^{2+} concentration increased. This is consistent with the understanding that Mg^{2+} could preferentially bind indirectly to the sugar-phosphate backbone.[36] The decrease of the peaks at ~1410 cm^{-1} (DNA base-sugar vibration) also suggested the same mechanism. At 10^{0} M, all the DNA assigned peaks disappeared and only that assigned to SO_4^{-2} was visible. This would be consistent with the speculation that there had been a precipitation event of $MgSO_4{\cdot}7H_2O$ which would have effectively shielded the target DNA.

The broad peaks at ~870 and 1069 cm^{-1} as well as the relatively sharper peaks at ~1350 and 1520 cm^{-1} were observed for magnetic beads (MB) only (Fig. 5a and b). Since the magnetic beads are super-paramagnetic with surface amine groups (NH_2) to allow for direct covalent binding with the carboxyl group on the quantum dots, the peaks at ~870 and 1520 cm^{-1} were unsurprising and readily attributed to N–H bending. However, the broad peak at 1069 cm^{-1} is attributed to C–N and C–O stretching modes, and the narrower peak at ~1350 cm^{-1} is attributed to C–H and O–H bending modes. It is possible that these peaks came from the additional undeclared formulation on the magnetic beads. Note that the exact

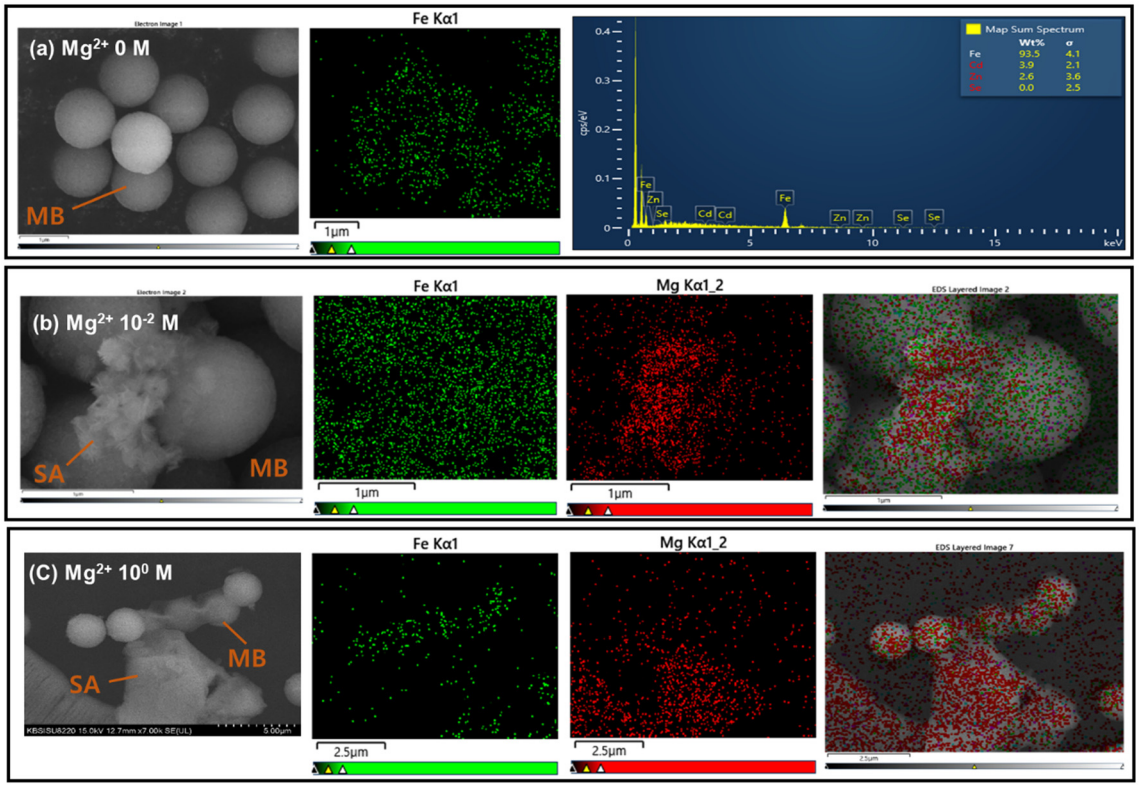

Fig. 3 FE-SEM and EDS layered images of MB-QD_{565}-probe DNA + QD_{655}-signaling DNA in the presence of Mg^{2+} ions of (a) 0 M, (b) 10^{-2} M, and (c) 10^{-0} M. Secondary aggregation is denoted as "SA".

formulation of the commercial magnetic beads is unknown and only the group intended for ligand binding is made known to the user (such as amine, streptavidin, epoxy, and carboxyl groups).

As expected, the covalent bonding with quantum dots (QD_{565}) reduced these peaks and it was consistent with the binding events between the amine group on the magnetic beads (MB) and the carboxyl group of the quantum dots (QD_{565}). Further conjugation with probe DNA further reduced these peaks. Upon the increase of Mg^{2+} from 10^{-4} to 10^{-2} M (Fig. 5c and d), the above-mentioned peaks further decreased. At this point, the amplitude reduction could be due to intra-complex interactions within the MB-QD_{565}-probe DNA complex (such as Mg^{2+} binding to other parts of the complex in addition to the probe DNA). It could also be due to non-specific aggregation between the MB-QD_{565}-probe DNA complex as a result of Mg^{2+} induced coulombic (electrostatic) attraction. However, it is only in the later scenario that Mg^{2+} could behave as a switchable inhibitor. The non-specific aggregation is also consistent with earlier FE-SEM and EDS observations in the presence of Mg^{2+} as shown in Fig. 2 and 3.

3.3. Non-specific binding of complexes due to Mg^{2+}

The fluorescence of MB-QD_{565}-probe DNA complex had decreased from 2585 ± 31 to 2389 ± 25 RFU as the Mg^{2+} concentration increased from 0 to 10^{0} M (Fig. 6a). Since it is not known that Mg^{2+} would result in the quenching or bleaching of QD_{565}, the decrease in fluorescence could be explained as a result of non-specific aggregation. In addition to the Mg^{2+} Coulomb attraction between the probe DNAs on the MB-QD_{565}-probe DNA complexes, the quantum dots were also known to aggregate as well in the presence of Mg^{2+}.[41] This is consistent with the zeta potential measurement results (Fig. 6b). Specifically, the zeta potential decreased from −44.0 ± 10.9 mV to −3.1 ± 2.7 mV as the Mg^{2+} concentration increased from 0 to 10^{0} M, which also suggested the possible aggregation.

Similarly, the fluorescence of the signaling DNA-QD_{655} complex also decreased from 24 852 ± 73 to 20 062 ± 38 RFU as the Mg^{2+} concentration increased from 0 to 10^{0} M (Fig. 6c). The zeta potential measurement is also evident of non-specific aggregation as it decreased from −37.2 ± 2.0 to −6.1 ± 2.1 RFU as the Mg^{2+} concentration increased from 0 to 10^{0} M.

Given the non-specific aggregation of complexes in the presence of Mg^{2+} (Fig. 6a–d), the fluorescence and zeta potential measurement results for MB-QD_{565}-probe DNA + signaling DNA-QD_{655} are no longer surprising. In the event of increased non-specific binding, the fluorescence ratio QD_{655}/QD_{565} would increase because more signaling DNA-QD_{655} complexes would bind to the MB-QD_{565}-probe DNA complexes. This would explain the increase in normalized fluorescence from

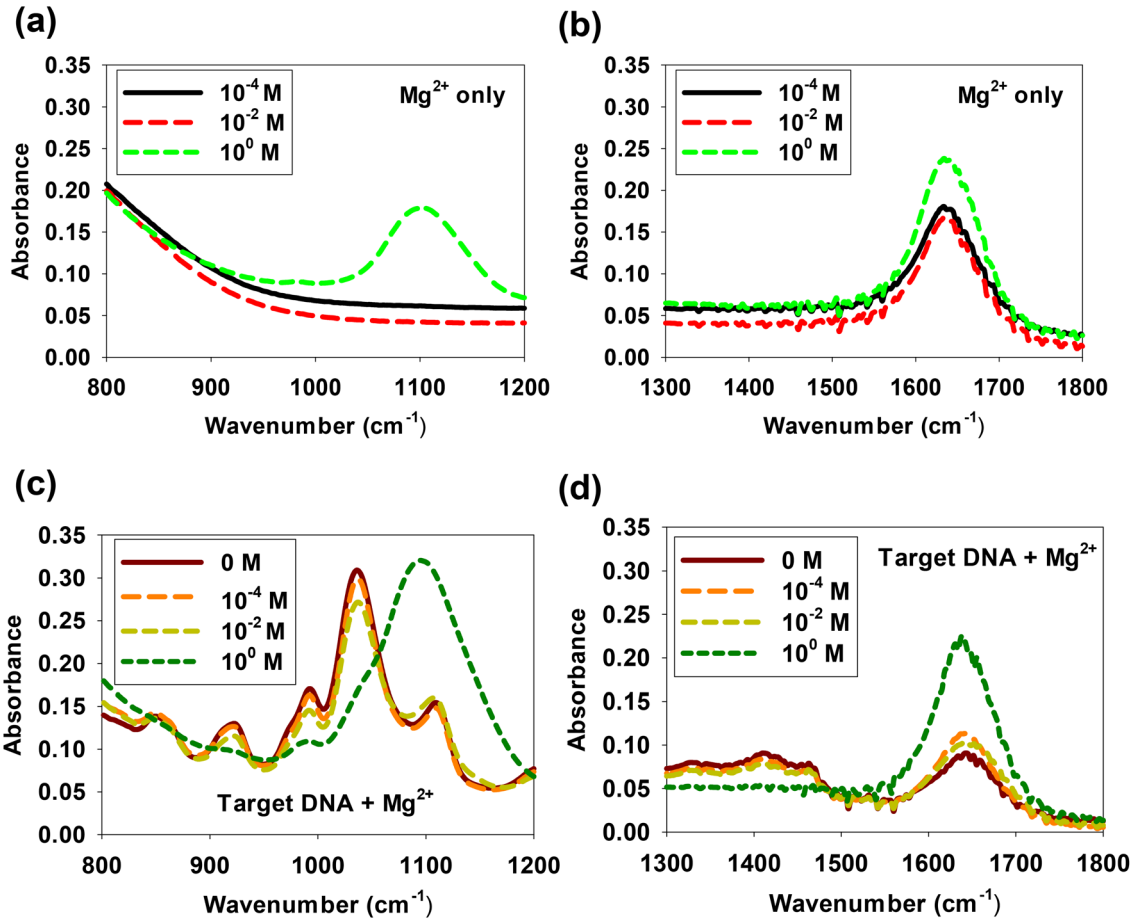

Fig. 4 FT-IR absorbance spectrum of (a) and (b) Mg^{2+} only, (c) and (d) target DNA, in the presence of 0, 10^{-4}, 10^{-2}, and 10^{0} M Mg^{2+}. The wavenumber from 800 to 1200 cm^{-1} was depicted in (a) and (c) and the wavenumber from 1300 to 1800 cm^{-1} was depicted in (b) and (d). The same description applies to Fig. 5.

0.203 ± 0.009 to 7.870 ± 0.260, and zeta potential from −40.7 ± 5.1 to −15.3 ± 0.5 mV, as Mg^{2+} increased from 0 to 10^{0} M.

3.4. Switchable inhibitory behavior of Mg^{2+} on gene quantification

The presence of 0, 10^{-5}, 10^{-4}, 10^{-3}, 10^{-2}, 10^{-1}, and 10^{0} M of Mg^{2+} resulted in the fluorescence ratio (QD_{655}/QD_{565}) of 0.77 ± 0.005, 0.70 ± 0.01, 0.68 ± 0.018, 2.18 ± 0.020, 4.95 ± 0.037, 4.09 ± 0.080, and 5.61 ± 0.065 RFU, respectively, for dsDNA (PCR amplicon) samples (Fig. 7a). It also resulted in the fluorescence ratio (QD_{655}/QD_{565}) of 0.91 ± 0.070, 0.62 ± 0.017, 0.57 ± 0.018, 1.99 ± 0.037, 4.83 ± 0.11, 2.37 ± 0.072, and 4.61 ± 0.210 RFU, respectively, for ssDNA samples.

The effect of Mg^{2+} on the fluorescence ratios for both dsDNA and ssDNA samples were similar. Both displayed initial quantification under-estimation at 10^{-5} and 10^{-4} M Mg^{2+} as compared to sample without inhibitor (0 M Mg^{2+}) followed by quantification over-estimation at Mg^{2+} concentration of 10^{-3} M and above. In order to appreciate the extent of quantification under- and over-estimation, the fluorescence ratio is converted to normalized fluorescence percentage as given by the following equation:

$$\text{Normalized fluorescence}\,\% = \frac{\text{Fluorescence at given } Mg^{2+} \text{ concentration}}{\text{Fluorescence in absence of } Mg^{2+}} \times 100. \quad (1)$$

In this case, using dsDNA samples, 10^{-5} and 10^{-4} M Mg^{2+} resulted in lower normalized fluorescence percentage at 90% and 88%, respectively (as compared to 100% for 0 M Mg^{2+}). Similarly, with ssDNA samples, 10^{-5} and 10^{-4} M Mg^{2+} resulted in lower normalized fluorescence percentage at 75% and 65%, respectively. Therefore, we demonstrated the manifestation of Mg^{2+} inhibition as quantification under-estimation which is consistent with the previous study.[21]

More importantly, as the inhibitor Mg^{2+} concentration reached 10^{-3} M or higher (10^{-3}, 10^{-2}, 10^{-1}, and 10^{0} M), the inhibition switched from under- to over-estimation. The corresponding normalized fluorescence percentage for dsDNA samples were exceedingly high at 283%, 643%, 532%, and 729%, respectively, as compared to that without inhibitor at

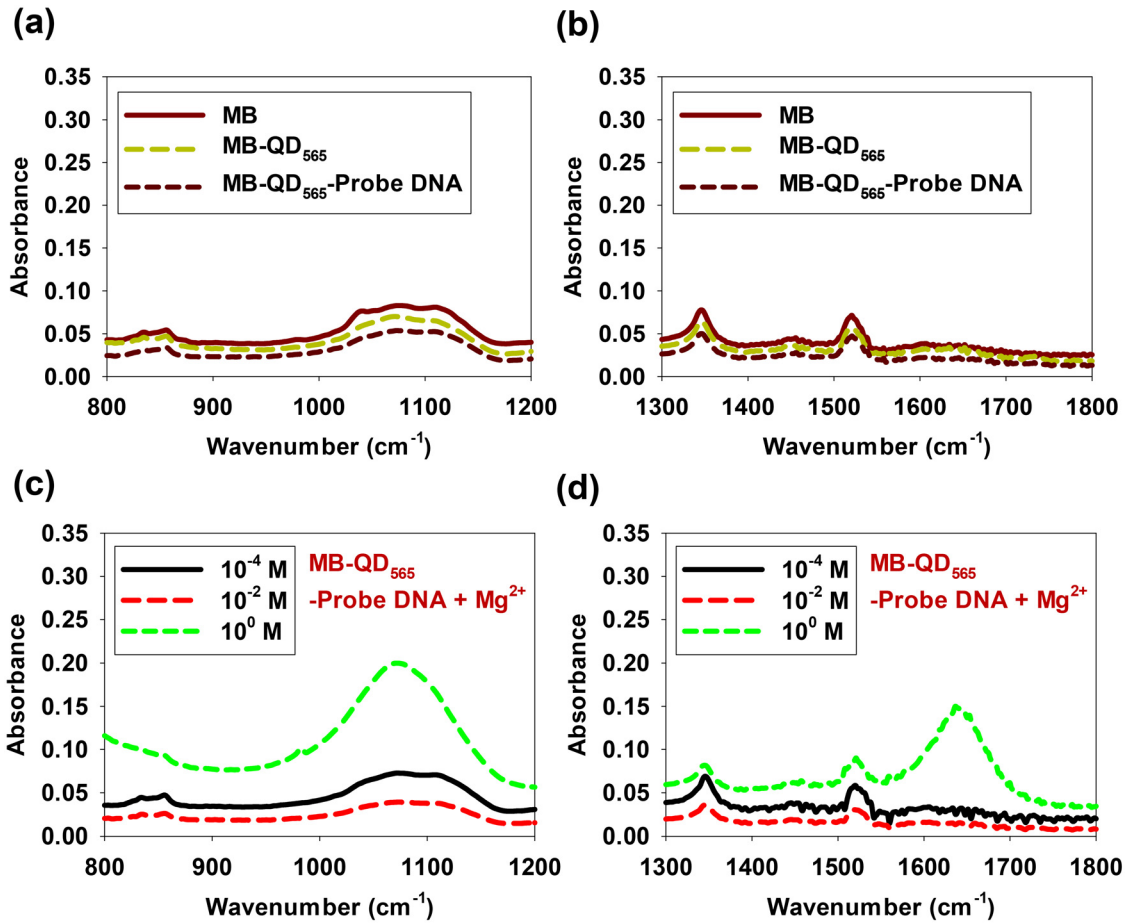

Fig. 5 FT-IR absorbance spectrum of (a) and (b) MB only, MB-QD_{565}, and MB-QD_{565}-probe DNA, (c) and (d) MB-QD_{565}-probe DNA in the presence of 10^{-4}, 10^{-2}, and 10^{0} M Mg^{2+}.

100% (0 M Mg^{2+}). Similarly, corresponding normalized fluorescence percentage for ssDNA samples were also exceedingly high at 218%, 531%, 260%, and 509%, respectively, as well. The inflection concentration of Mg^{2+} in this case is ~10^{-3} M.

3.5. Comparison with the inhibitory behavior of Cu^{2+} and Ca^{2+}

In order to contrast the inhibitory behavior between different cations more effectively, normalized fluorescence percentage is also employed instead of fluorescence ratios (with ssDNA as target DNA) (Fig. 7b). For inhibitor Ca^{2+} concentrations of 10^{-5}, 10^{-4}, 10^{-3}, 10^{-2}, 10^{-1}, and 10^{0} M, the normalized fluorescence percentage yielded 74 ± 3, 74 ± 8, 63 ± 2, 3 ± 1, 0 ± 0, and 4 ± 0%, respectively. It is noted that the dotted line depicts 100%, which represents the absence of inhibitors. Similarly, for inhibitor Cu^{2+} at the same concentrations, the normalized fluorescence percentage yielded 88 ± 9, 61 ± 10, and 0% thereafter. This shows that both Cu^{2+} and Ca^{2+} behaved as singular inhibitors (quantification under-estimation) throughout the entire concentration range of 10^{-5} to 10^{0} M. Furthermore, as the inhibitor concentration increased, the quantification under-estimation became more significant. This is consistent with the understanding that both Cu^{2+} and Ca^{2+} could form direct binding with the target DNA, probe DNA as well as signaling DNA to prevent DNA hybridization.

On the other hand, quantification under-estimation only occurred for Mg^{2+} at lower concentrations of 10^{-5} and 10^{-4} M. They yielded the normalized fluorescence percentage of 91 ± 2, 88 ± 3%, respectively. However, at higher Mg^{2+} concentrations of 10^{-3}, 10^{-2}, 10^{-1}, and 10^{0} M, quantification over-estimation was observed expectedly with normalized fluorescence percentages of 283 ± 2, 643 ± 8, 532 ± 14, and 729 ± 10%, respectively. Therefore, quantification over-estimation was only observed for Mg^{2+} but not for Ca^{2+} and Cu^{2+}.

Mechanism behind the inhibition by Ca^{2+} and Cu^{2+}. Hydrated Ca^{2+} (coordination number = 6–8, water–oxygen distance = 2.3–3.4 Å) has a flexible first solvation shell and is therefore more likely to form a direct bond with the DNA base pair. Specifically, the hydrated cations can directly or indirectly bind (*via* hydrogen bond with the water molecules of the first solvation shell) to the DNA's phosphate backbone as well as major groove at the guanine–cytosine base pairs.[42] Once the cation binds to the DNA, it will render it inaccessible for DNA

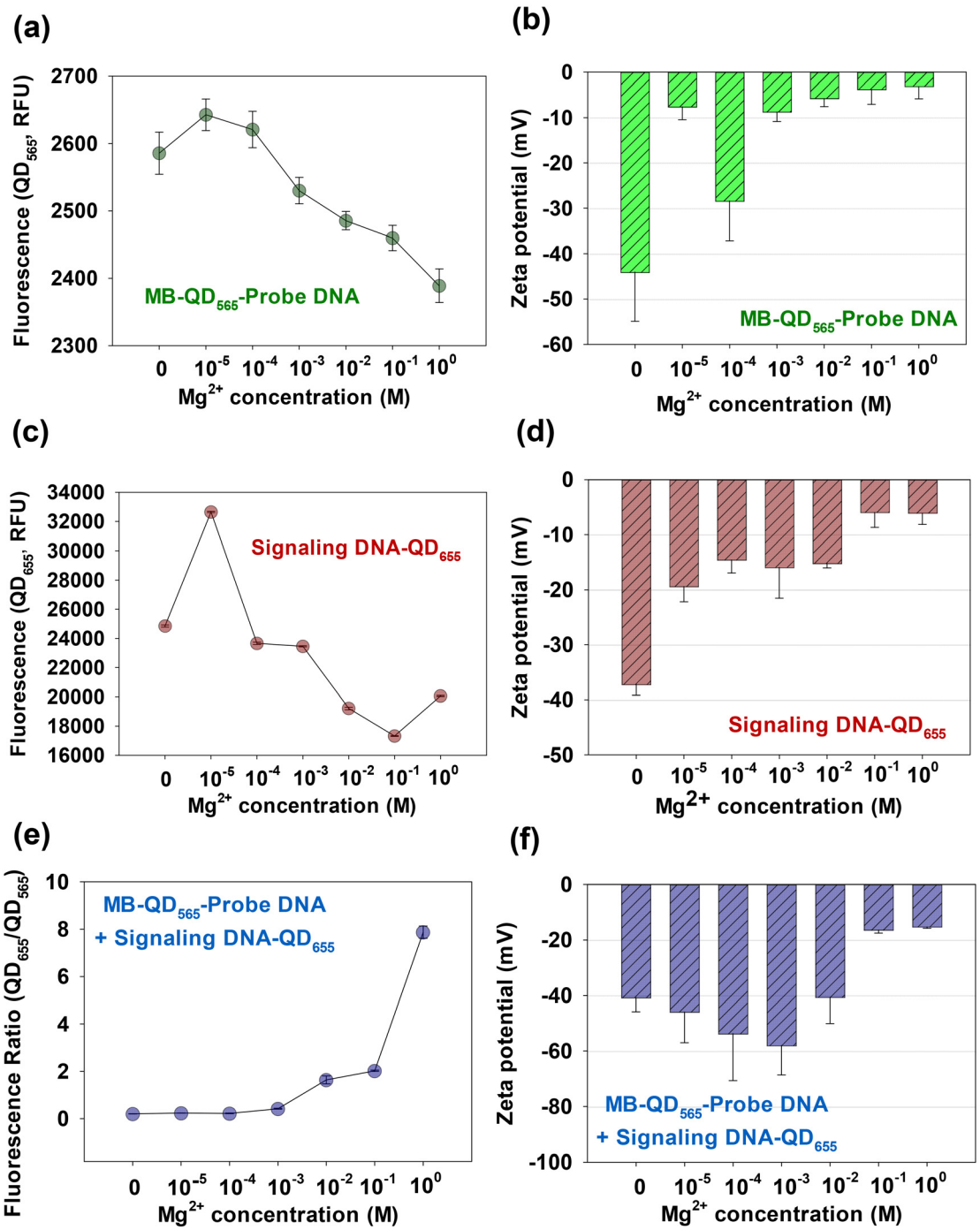

Fig. 6 In the presence of Mg^{2+} at varying concentrations, (a) QD_{565} fluorescence change of MB-QD_{565}-probe DNA. (b) Zeta potential change of MB-QD_{565}-probe DNA. (c) QD_{655} fluorescence of signaling DNA-QD_{655}. (d) Zeta potential change of signaling DNA-QD_{655}. (e) QD_{565}/QD_{655} fluorescence change of MB-QD_{565}-probe DNA + signaling DNA-QD_{655} in the absence of target DNA. (f) Zeta potential change of MB-QD_{565}-probe DNA + signaling DNA-QD_{655} in the absence of target DNA.

hybridization with another DNA. It is also possible that Ca^{2+} and Cu^{2+} bind strongly to the guanine bases, which stresses the DNA structure and results in the denaturation of the G–C pair of DNA.[43,44] In either scenario, the hybridization between the target DNA and the probe as well as signaling DNAs is compromised. More importantly, the inhibition in this case will only result in under-estimation with a corresponding lower fluorescence ratio QD_{655}/QD_{565}.

Mechanism behind Mg^{2+} switchable inhibitory behavior. The switchable inhibitory behavior of Mg^{2+} could be attributed to its well-defined and rigid first solvation shell (coordination number = 6, water–oxygen distance = 1.8–2.3 Å).[42] This means

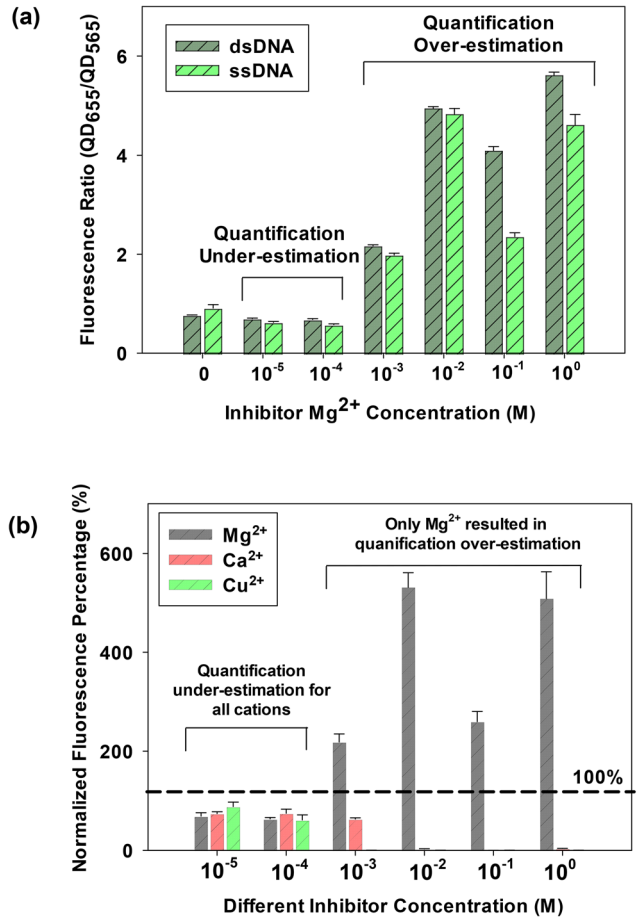

Fig. 7 (a) Switchable inhibitory behavior of Mg^{2+} on the NanoGene assay with ssDNA and dsDNA as target DNA. (b) Comparison of inhibitory behavior of Ca^{2+} and Cu^{2+} with the switchable inhibitory behavior of Mg^{2+} on the NanoGene assay.

it does not easily change its structure to accommodate direct binding between the cation and the DNA base pair. Given the smaller ionic radius of Mg^{2+}, it is reasonable to assume the dominance of Coulomb forces (*i.e.*, electrostatic force) in the interaction between Mg^{2+} and DNA. With large enough quantities of Mg^{2+}, the Coulomb forces may be sufficiently large to cause non-specific binding between the probe DNA and signaling DNA in the absence of the target DNA in the NanoGene assay. In other words, Mg^{2+} could mimic the presence of the target DNA at these high concentrations. Therefore Mg^{2+} was able to behave like a switchable inhibitor, where it can cause both under- and over-estimation at low and high concentrations, respectively.

3.6. Limitations and implications of the study

The maximum environmentally relevant concentrations for Mg^{2+}, Ca^{2+} and Cu^{2+} are approximately in the range 10^{-3} M. For example, the Mg^{2+} concentrations in aquatic and soil samples ranges from 4–212 and 10–528 mg L^{-1} (1.7×10^{-4}–8.7×10^{-3} and 4.1×10^{-4}–2.2×10^{-3} M), respectively.[12,45,46] Its concentration range in tap water is 5–29 mg L^{-1} (2.1×10^{-4}–1.2×10^{-3}). Similarly, the Cu^{2+} concentration in water ranges from 0.001–69 mg L^{-1} (or 1.5×10^{-8}–1.1×10^{-3} M).[45,47,48] In the soil environment, Ca^{2+} concentration is in the range of 27–934 mg L^{-1} (or 0.7×10^{-3}–23.3×10^{-3} M),[49] while that of Cu^{2+} is 3×10^{-3}–135×10^{-3} mg L^{-1} (or 0.1×10^{-6}–2.1×10^{-6} M) as soluble contents.[50] This means that environmentally relevant concentration range of these cations straddles across the two distinct regions that correspond to Mg^{2+} induced quantification under- and over-estimation, respectively (Fig. 7a and b).

In this study, the experiments were limited to the samples containing single cations. As shown in Fig. 7b, however, it is possible that the co-existence of Mg^{2+} with Ca^{2+} and Cu^{2+} in the sample can result in a fluorescence superposition due to the different preferences in DNA binding sites. For example, the presence of Ca^{2+} and Cu^{2+} will restrict the direct binding between the complexes (DNA hybridization), while Mg^{2+} will encourage indirect binding *via* Coulomb attraction. In this case, the end result could be either quantification under- or over-estimation and it depends on the relative quantities of Mg^{2+}, Ca^{2+}, and Cu^{2+} in the samples.

Last but not least, it is entirely possible that the inflection concentration of Mg^{2+} is dependent on the structure of the target, probe and signaling DNAs. In this case, it may be necessary to re-characterize the impact of switchable inhibitors on the assay results for a given target DNA. Strategies for re-characterization can include molecular modeling or performing the NanoGene assay for the new target DNA.[51–53] For example, in this study, the Mg^{2+} inflection concentration has been identified for *mcy*D gene (specific to *Microcystis aeruginosa*). Similarly, that for other environmental relevant bacteria such as *E. coli* can be determined *via* the same experiment. Since users often have a specific bacterial gene of interest, it is entirely feasible to employ the protocol presented in this study to establish the inflection concentration for that particular gene.

4. Conclusions

We have discovered that the divalent cation Mg^{2+} behaves like a switchable inhibitor in a gene quantification assay (NanoGene assay). At low concentrations, it caused quantification under-estimation like other common environmental inhibitors such as Ca^{2+} and Cu^{2+}. However, at high concentrations, Mg^{2+} switched to cause quantification over-estimation. The crux of this discovery lies in the inflection concentration of $\sim 10^{-3}$ M which is well within the environmentally relevant concentrations of Mg^{2+}. In other words, in the context of environmental monitoring of a specific target gene, a false positive can be induced because of elevated Mg^{2+}. In the broader context, the spatial and temporal fluctuation in Mg^{2+} concentrations in environmental samples can render any gene monitoring efforts utterly inaccurate and counter-intuitive. Fortunately, users are often only required to monitor for specific gene in the samples. Coupled with Mg^{2+} measurement, it will be feasible to compensate for either under or

over-estimation for that specific gene once it has been characterized. Therefore, it will be useful to identify the Mg^{2+} inflection concentrations for other commonly targeted genes in environmental samples as part of the future work.

Conflicts of interest

There are no conflicts to declare.

Acknowledgements

This study was supported by the National Research Foundation of Korea (NRF-2019R1A2C2084233).

References

1 D. A. Hutchins, J. K. Jansson, J. V. Remais, V. I. Rich, B. K. Singh and P. Trivedi, *Nat. Rev. Microbiol.*, 2019, **17**, 391–396.
2 R. Cavicchioli, W. J. Ripple and N. S. Webster, *Nat. Rev. Microbiol.*, 2019, **17**, 569–586.
3 P. Gwimbi, M. George and M. Ramphalile, *Environ. Health Prev. Med.*, 2019, **24**, 33–39.
4 S. M. Hermans, H. L. Buckley, B. S. Case, F. Curran-Cournane, M. Taylor and G. Lear, *Microbiome*, 2020, **8**, 79.
5 E.-H. Lee, B. Chua and A. Son, *Environ. Sci. Technol.*, 2018, **52**, 1375–1385.
6 G.-Y. Kim and A. Son, *Anal. Chim. Acta*, 2010, **677**, 90–96.
7 X. Wang, M. R. Liles and A. Son, *Soil Biol. Biochem.*, 2013, **58**, 9–15.
8 E. A. Barlaan, S. Furukawa and K. Tekeuchi, *Environ. Microbiol.*, 2006, **9**, 690–702.
9 R. Benner, *Nat. Rev. Microbiol.*, 2011, **9**, 75.
10 X. Wang, B. Chua and A. Son, *Sensors*, 2018, **18**, 2646–2655.
11 G.-Y. Kim, X. Wang and A. Son, *J. Environ. Monit.*, 2011, **13**, 1344–1350.
12 X. Wang, H. Kweon, S. Lee, H. Shin, B. Chua, M. R. Liles, M.-K. Lee and A. Son, *Soil Biol. Biochem.*, 2018, **125**, 300–308.
13 H. Gong, Y. Wu, R. Zeng, Y. Zeng, X. Liu and D. Tang, *Chem. Commun.*, 2021, **57**, 8977–8980.
14 R. Zeng, H. Gong, Y. Li, Y. Li, W. Lin, D. Tang and D. Knopp, *Anal. Chem.*, 2022, **94**, 7442–7448.
15 C. S. Jacobsen and O. F. Rasmussen, *Appl. Environ. Microbiol.*, 1992, **58**, 2458–2462.
16 I. G. Wilson, *Appl. Environ. Microbiol.*, 1997, **63**, 3741–3751.
17 R. J. Steffan, J. Goksoyr, A. K. Bej and R. M. Atlas, *Appl. Environ. Microbiol.*, 1988, **54**, 2908–2915.
18 E. W. Alm, D. Zheng and L. Raskin, *Appl. Environ. Microbiol.*, 2000, **66**, 4547–4554.
19 D. S. Bachoon, E. Otero and R. E. Hodson, *J. Microbiol. Methods*, 2001, **47**, 73–82.
20 G. Kim, X. Wang and A. Son, *J. Environ. Monit.*, 2011, **13**, 1344–1350.
21 H. Jin, Y. Yoon, M. R. Liles, B. Chua and A. Son, *Analyst*, 2020, 6846–6858.
22 E.-H. Lee, K.-S. Cho and A. Son, *J. Microbiol. Biotechnol.*, 2017, **27**, 808–815.
23 E.-H. Lee, B. Chua and A. Son, *Biosens. Bioelectron.*, 2016, **83**, 205–212.
24 E.-H. Lee, H. J. Lim, A. Son and B. Chua, *Analyst*, 2015, **140**, 7776–7783.
25 K. A. Mitchell, B. Chua and A. Son, *Biosens. Bioelectron.*, 2014, **54**, 229–236.
26 P. A. Krieg, *A laboratory guide to RNA: Isolation, analysis, and synthesis*, John Wiley & Sons, Inc., 1996.
27 H.-M. Oh, S. J. Lee, M.-H. Jang and B.-D. Yoon, *Appl. Environ. Microbiol.*, 2000, **66**, 176–179.
28 J. M. Rinta-Kanto, A. J. Ouellette, G. L. Boyer, M. R. Twiss, T. B. Bridgeman and S. W. Wilhelm, *Environ. Sci. Technol.*, 2005, **39**, 4198–4205.
29 X. Wang and A. Son, *Environ. Sci.: Processes Impacts*, 2013, **15**, 2204–2212.
30 A. R. Tuama and T. M. Al-Saadi, *Energy Procedia*, 2019, **157**, 709–718.
31 F. Ovalles, M. Gallignani, R. Rondon, M. Brunetto and R. Luna, *Lat. Am. J. Pharm.*, 2009, **28**, 173–182.
32 M. Dhandapani, L. Thyagu, P. Arun Prakash, G. Amirthaganesan, M. A. Kandhaswamy and V. Srinivasan, *Cryst. Res. Technol.*, 2006, **4**, 328–331.
33 J. Coates, Interpretation of infrared spectra, a practical approach, in *Encyclopedia of analytical chemistry*, ed. R. A. Meyers, John Wiley & Sons, 2006.
34 L.-J. Zhao, Y.-H. Zhang, Z.-F. Wei, H. Cheng and X.-H. Li, *J. Phys. Chem.*, 2006, **3**, 951–958.
35 H. A. Tajmir-Riahi, M. Naoui and R. Ahmad, *Biopolymers*, 1993, **33**, 1819–1827.
36 K. Serec, S. Babić, R. Podgornik and S. Tomić, *Nucleic Acids Res.*, 2016, **44**, 8456–8464.
37 B. R. Wood, *Chem. Soc. Rev.*, 2016, **45**, 1980–1998.
38 M. L. S. Mello and B. C. Vidal, *PLoS One*, 2012, **7**, e43169.
39 M. Banyay, M. Sarkar and A. Gräslund, *Biophys. Chem.*, 2003, **104**, 477–488.
40 R. Ahmad, M. Naoui, J. F. Neault, S. Diamantoglou and H. A. Tajmir-Riahi, *J. Biomol. Struct. Dyn.*, 1996, **13**, 795–802.
41 C.-Y. Zhang and D. Li, *Analyst*, 2010, **135**, 2355–2359.
42 M. P. Long, S. Alland, M. E. Martin and C. M. Isborn, *Phys. Chem. Chem. Phys.*, 2020, **22**, 5584–5596.
43 H. Richard, J. P. Schreiber and M. Daune, *Biopolymers*, 1973, **12**, 1–10.
44 R. Ahmad, H. Arakawa and H. A. Tajmir-Riahi, *Biophys. J.*, 2003, **84**, 2460–2466.
45 A. N. Amadi, J. Yisa, I. C. Ogbonnaya, M. A. Dan-Hassan, J. O. Jacob and Y. B. Alkali, *J. Geography Geology*, 2012, **4**, 13–21.
46 A. Kuriata-Potasznik and S. Szymczyk, *J. Elem.*, 2015, **20**, 677–692.
47 U. Rösner, *Environ. Geol.*, 1998, **33**, 224–230.

48 J. S. Reed and J. C. Henningson, *J. - Am. Water Works Assoc.*, 1984, **76**, 60–65.
49 J. Johnstone and S. Kokelj, *Arctic*, 2008, **61**, 199–211.
50 I. N. Pais and J. Benton Jones, *The handbook of trace elements*, St. Lucie Press, Boca Raton, Fla., 1997.
51 M. Yoosefian, E. Mirhaji, M. Afshar and A. Juan, *Appl. Surf. Sci.*, 2020, 146572.
52 I. Jeddi and L. Saiz, *Sci. Rep.*, 2017, **7**, 1178.
53 A. Krüger, F. M. Zimbres, T. Kronenberger and C. Wrenger, *Biomolecules*, 2018, **8**, 83.